High Accuracy and Low Complexity Frequency Offset Estimation Method Based on All Phase FFT for M-QAM Coherent Optical Systems

Qian Li , Aiying Yang , Peng Guo , and Xiangjun Xin

Abstract—The traditional fast Fourier transform based frequency offset estimation (FFT-FOE) estimates the frequency offset by searching the spectral peak of the signal after the fourth power operation, which is suitable for multiple modulation formats. But the accuracy of FOE is limited by the number of FFT points. In this paper, we propose a high accuracy and low complexity FOE algorithm based on all phase FFT (APFFT-FOE). The accuracy of FOE can be improved effectively with lower additional computational complexity. Simulation results show that the mean square error of APFFT-FOE is reduced by more than one order of magnitude compared with the FFT-FOE. Compared with other FOE algorithms that can achieve the same accuracy, the additional computational complexity required by APFFT-FOE is reduced by more than 50%. Finally, the APFFT-FOE is experimentally verified with 20 GBaud 16/64-QAM modulation signal. The experimental results show that the required OSNR for 16-QAM signal to reach 6.7% hard-decision forward-error correction is relaxed by 0.23 dB. For 64-QAM signal, the required OSNR at 20% soft-decision forward-error correction threshold is relaxed by 0.68 dB.

Index Terms—Frequency offset estimation, all phase FFT, coherent communication.

I. INTRODUCTION

DUE to the booming development of bandwidth-hungry services such as 5 G and cloud, optical network is developing towards large capacity, high spectrum efficiency and flexible architectures [1], [2]. In coherent optical communication systems, M-ary quadrature amplitude modulation (M-QAM) together with digital signal processing (DSP) is the main solution to achieve such goal [3]–[5]. In the DSP flow of coherent receiver, the frequency offset estimation (FOE) is a key step to compensate for the frequency mismatch between the transmitter laser and the local oscillator (LO) [6].

Qian Li, Aiying Yang, and Peng Guo are with the Key Laboratory of Photonics Information Technology, Ministry of Industry and Information Technology, School of Optics and Photonics, Beijing Institute of Technology, Beijing 100081, China (e-mail: 3120190539@bit.edu.cn; yangaiying@bit.edu.cn; guopeng0304@bit.edu.cn).

Xiangjun Xin is with the School of Electronic Engineering, Beijing University of Posts and Telecommunications, Beijing 100876, China (e-mail: xjxin@bupt.edu.cn).

In high symbolrate coherent optical communication systems, a feed-forward and non-data-aided FOE algorithm is more preferred. Up to now, a various of non-data-aided FOE schemes have been proposed [7]–[13]. The differential phase based FOE (diff-FOE) is widely used in M-ary phase shift keying (M-PSK) modulation systems [7], which can also be apllied to 16-QAM combining with QPSK partition method [8], [9]. However, when it is used for higher order QAM (e.g., 32-QAM and 64-QAM), complicated partition and rotation operations are required for constellation points [10], [11]. In general, diff-FOE cannot be applied to multiple modulation formats easily, and usually requires a long symbols of more than 10000 to ensure the accuracy of FOE, which is not conducive to fast tracking of frequency offset. Another FOE algorithm based on fast Fourier transform of signal with fourth-power (FFT-FOE) is suitable for a variety of modulation formats (e.g., QPSK and 8/16/64-QAM) [12], and can also be applied to the 32-QAM by amplifying the inner QPSK constellation points [13]. FFT-FOE can achieve fast frequency offset estimation within hundreds of symbols. Moreover, due to the frequency offset estimation implement in the frequency domain, FFT-FOE has the advantage of high ASE noise tolerance. However, since the computational complexity of FFT increases rapidly with FFT size, FFT-FOE is usually performed with a short block of symbols in real-time implementation, for example, 512 symbols [12] and 528 symbols [14] for 16-QAM. In this case, the frequency offset estimation accuracy of FFT-FOE is limited. Thus, the two-stage FOE algorithms are proposed. On the basis of FFT-FOE with fewer symbols in the first stage, the two-stage FOE algorithms performed a more accurate frequency offset estimation in the second stage based on the chirp z-transform (CZT) [15], Zoom-FFT [16] or spectral interpolation method (IpDFT) [17]. This structure can reduce the overall complexity while maintaining a high-precision frequency offset estimation. but the complexity caused by CZT or Zoom-FFT is still high, As for the spectral interpolation method, it requires discrete time Fourier transform (DTFT) in many cases, which also leads to higher computational complexity.

In this paper, we propose a high accuracy and low complexity FOE algorithm based on all phase FFT (APFFT-FOE). APFFT has advantages of suppressing spectrum leakage and high precision of phase estimation compared with conventional FFT [18]. Based on the phase characteristics of APFFT, APFFT-FOE can correct the estimated frequency offset using the APFFT phase

spectrum of signal with very low additional complexity consuming compared with FFT-FOE. Simulation results show that the mean square error of APFFT-FOE is reduced by more than one order of magnitude compared with FFT-FOE. However, the additional computational complexity of APFFT-FOE is reduced by 87%, 74% and 50 % compared with the CZT, Zoom-FFT and IpDFT based algorithms, respectively. Finally, the proposed APFFT-FOE is experimentally verified under B2B transmission using 20 GBaud 16/64-QAM modulation. The experimental results show that the required OSNR for 16-QAM signal to reach 6.7% hard-decision forward-error correction (HD-FEC) is relaxed by 0.23 dB. For 64-QAM signal, the required OSNR at 20% soft-decision forward-error correction (SD-FEC) threshold is relaxed by 0.68 dB.

II. ALL PHASE FFT BASED FREQUENCY OFFSET ESTIMATION

In coherent receiver, the received M-QAM signal before FOE can be modeled as [12]

$$S_n = m_n \exp\left[j(2\pi f_d n T_s + \varphi_n)\right] + N_n \tag{1}$$

where m_n is the n-th modulated data of M-QAM, f_d is the frequency offset (FO), T_s represents the symbol duration, φ_n denotes the Wiener process phase noise, and N_n is the Gaussian distributed ASE noise. For traditional FFT-FOE, FO is estimated based on the peak search in the magnitude spectrum of the signal after the fourth power operation, which can be described as below

$$\hat{f}_d = \frac{1}{4} \arg \max_{f \in [-R_s/2, R_s/2]} \left| \frac{1}{L} \sum_{k=0}^{L-1} S_n^4 e^{-j2\pi f k T_s} \right| \tag{2}$$

where R_s represents the sampling rate, and L is the length of a frame of signal to obtain the spectrum. The time-frequency conversion of the signal is usually carried out by FFT technique.

Without considering the influence of laser phase noise and ASE noise on the signal spectrum, the FFT spectrum of the signal after the fourth power operation (denoted by S_n^4) can be expressed as [17]

$$Y(k) = A \frac{\sin[\pi(F-k)]}{\sin[\pi(F-k)/L]} e^{[j\pi(F-k)(L-1)/L]},$$
$$k = 0, 1, 2, \ldots, L-1 \tag{3}$$

where F is the normalized FO, which can be divided into integer part k_d and decimal part δ ($-0.5 < \delta \leq 0.5$), defined as

$$F/L = 4f_d T_s = (k_d + \delta)/L \tag{4}$$

From (3), the spectral component with the largest amplitude is $\hat{k} = k_d$. Therefore, the theoretical value of FO estimated by FFT-FOE can be expressed as

$$\hat{f}_d = \frac{1}{4}\hat{k} \cdot \Delta f_{\text{res}} \tag{5}$$

where Δf_{res} is the spectral resolution (defined as R_s/L). Obviously, FFT-FOE can only estimate k_d (the integer part of F), but the decimal part δ can not be obtained duo to the picket-fence effect of FFT. Therefore, the accuracy of FOE is limited by the spectral resolution. On the basis of FFT-FOE, the two-stage
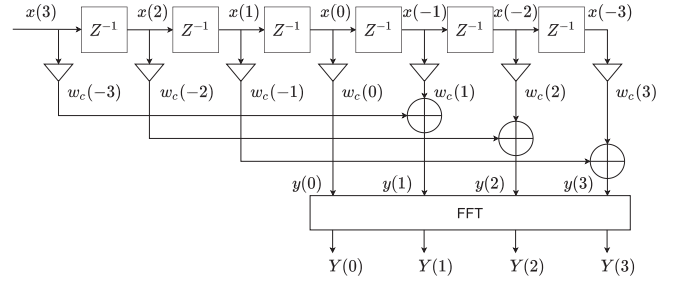

Fig. 1. Schematic diagram of APFFT spectral analysis (in the case of $L=4$).
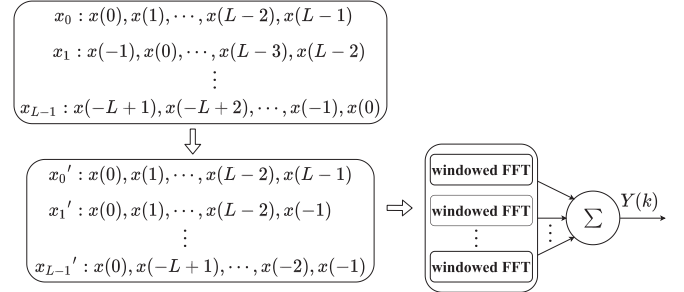

Fig. 2. Relationship between all phase FFT and traditional windowed FFT.

FOE algorithms can proceed a more accurate FO estimation, however, the complexity required for the second stage is still relatively high.

In order to further reduce complexity, we propose the all phase FFT based FOE. APFFT is a derivative method of FFT. Fig. 1 shows the schematic diagram of APFFT [18], which includes two steps of signal preprocessing and FFT. In the signal preprocessing step, the fixed real convolution window (denoted by $w_c(n)$, $-L+1 \leq n \leq L-1$) is used to weight the signal $x(n)$, $-L+1 \leq n \leq L-1$, then, we obstain the all phase signal $y(n)$ by adding the two signals with an interval of L in the weighted signal. Finally, the APFFT spectrum of $x(n)$ can be obtain by implementing FFT on $y(n)$.

Fig. 2 shows the relationship between APFFT and traditional windowed FFT [19]. The signals with a length of L and containing $x(0)$ are denoted as x_m, which can be expressed as

$$x_m(n) = x(-m+n), \quad m, n = 0, 1\cdots, L-1 \tag{6}$$

x'_m is the signal that rotates x_m to the left by m symbols, with the first place being $x(0)$. The APFFT spectrum of $x(n)$, $-L+1 \leq n \leq L-1$ is equivalent to implement windowed FFT for all x'_m and summing it up.

Therefore, according to the cyclic shift property of FFT, the APFFT spectrum of S_n^4, $-L+1 \leq n \leq L-1$ can be expressed as

$$Y_{\text{ap}}(k) = \frac{1}{L} \sum_{m=0}^{L-1} Y'_m(k)$$
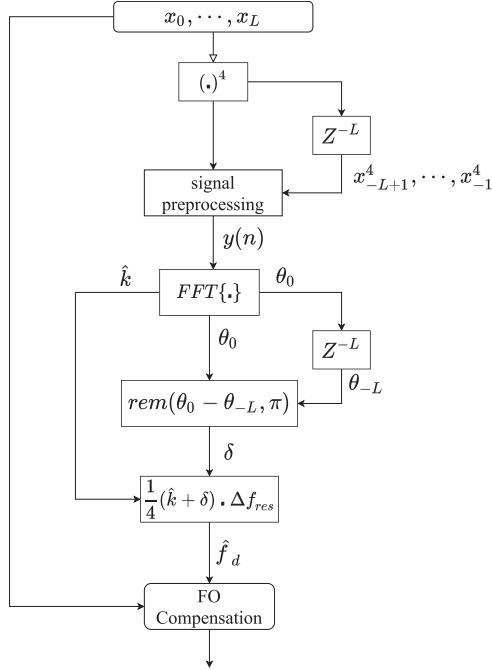$$= \frac{1}{L} \sum_{m=0}^{L-1} Y_m(k) e^{j2\pi mk/L}$$

Fig. 3. Block diagram of APFFT-FOE scheme.

$$= [A\frac{\sin[\pi(F-k)]}{\sin[\pi(F-k)/L]}]^2 e^{j\theta_0},$$
$$k = 0, 1, 2, \ldots, L-1 \qquad (7)$$

where θ_0 represents the theoretical phase of the central symbol of S_n^4. From (7) and (3), we can see that the amplitude of the APFFT spectrum of S_n^4 is the square of the traditional FFT spectrum. Therefore, the FO can also be obtained based on the position of the peak in APFFT spectrum, which has the same expression as (5). On the other hand, the phase at the peak of the APFFT spectrum can reflect the signal phase well. Taking the previous block of signal (i.e. S_n^4, $-2L+1 \leq n \leq -1$) into account, the phase at the peak of the APFFT spectrum is θ_{-L}. Due to the influence of FO, there is a relationship between θ_0 and θ_{-L} as shown below

$$\theta_0 = \theta_{-L} + 2\pi \cdot 4f_d T_s L \qquad (8)$$

Based on (4) and (8), an estimation of δ can be obtained as

$$\delta \cdot 2\pi = \text{rem}(\theta_0 - \theta_{-L}, \pi) \qquad (9)$$

where $\text{rem}(A, B)$ represents for the remainder operation. Finally, the FO estimated by APFFT-FOE can be expressed as

$$\hat{f}_d = \frac{1}{4}(\hat{k} + \delta) \cdot \Delta f_{\text{res}} \qquad (10)$$

The block diagram for APFFT-FOE is shown in Fig. 3. It should be noted that the signal in the previous block is only used for signal preprocessing, so as to obtain the all phase signal $y(n)$.

III. SIMULATION RESULTS

To investigate the performance of APFFT-FOE, we carried out simulations for 28 GBaud 16/64-QAM based coherent system.
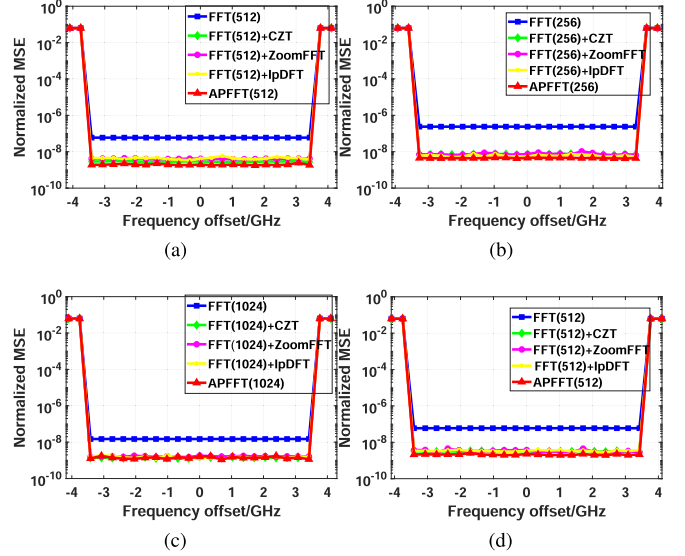

Fig. 4. Normalized MSE versus frequency offset for (a), (b) 16-QAM and (c), (d) for 64-QAM.

The linewidth of transmitter laser and LO are both set to be 100 kHz. At the coherent receiver side, the traditional FFT-FOE and the two-stage FOE based on CZT, Zoom-FFT and IpDFT are also implemented. To compare the performance of different FOE schemes fairly, we choose the FFT size (denoted by N_1) in FFT-FOE or APFFT-FOE as 512/256 for 16-QAM and 1024/512 for 64-QAM, which is the same with the first step of the two-stage FOE. In the second step, the Zoom-FFT size (denoted by N_2) is set to be $N_1/2$, or M-point CZT of N_3 signals is implemented ($M = 32$, $N_3 = N_1 - M + 1$) [15].

Fig. 4 depict the normalized mean square error (MSE, defined as $E|(\hat{f}_d - f_d)T_s|^2$) of different FOE schemes versus the FO for 16/64-QAM. The SNR is set to be 20 dB. For each measurement of the MSE, the results are obtained over 1000 independent simulations. All the FOE schemes have the same estimated range of [-symbol rate/8, +symbol rate/8], i.e. $[-3.5$ GHz, $+3.5$ GHz] for 28 GBaud 16/64-QAM. The FFT-FOE always has a residual FO of $\frac{1}{8}\Delta f_{\text{res}}$ at the selected FO due to the picket-fence effect of FFT. However, the APFFT-FOE and the two-stage FOE can significantly reduce the residual FO. For 16/64-QAM signals, the MSE obtained by FFT-FOE is 6e-8/1.5e-8 when FFT size is set to 512/1024, while APFFT-FOE decrease it to 1.9e-9/1.4e-9. When FFT size is reduced to 256/512, the MSE of FFT-FOE increases to 2.4e-7/6e-8 due to the reduced spectral resolution, while the MSE obtained by APFFT only increases to 4.5e-9/2e-9. This means that APFFT-FOE can mitigate the increase of residual FO caused by the reduction of spectral resolution, which will make sense when the FFT size is strictly limited in modern high-speed transponders due to the computational complexity reason.

To show the effect of ASE noise on APFFT-FOE, Fig. 5 depict the MSE as a function of SNR for 16/64-QAM. The FO is chosen in the range [-3.5 GHz, +3.5 GHz] with an interval of 200 MHz, therefore, the MSE under each SNR is obtained by over 36000 independent simulations. The Cramer-Rao lower
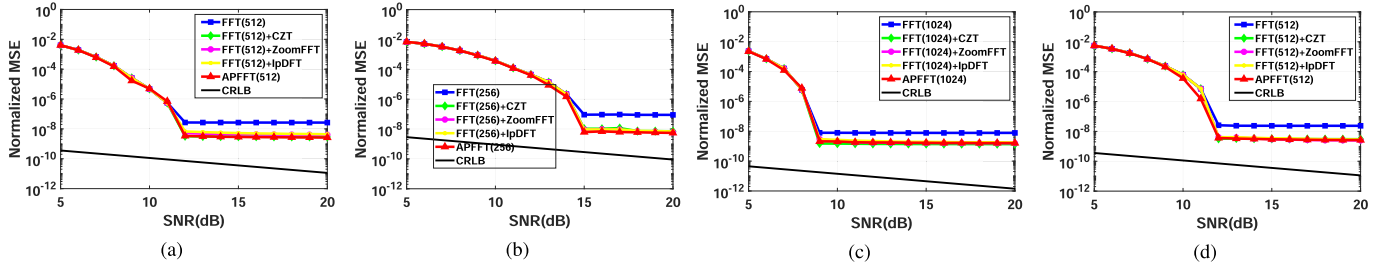
Fig. 5.   Normalized MSE versus SNR for (a), (b) 16-QAM and (c), (d) for 64-QAM.
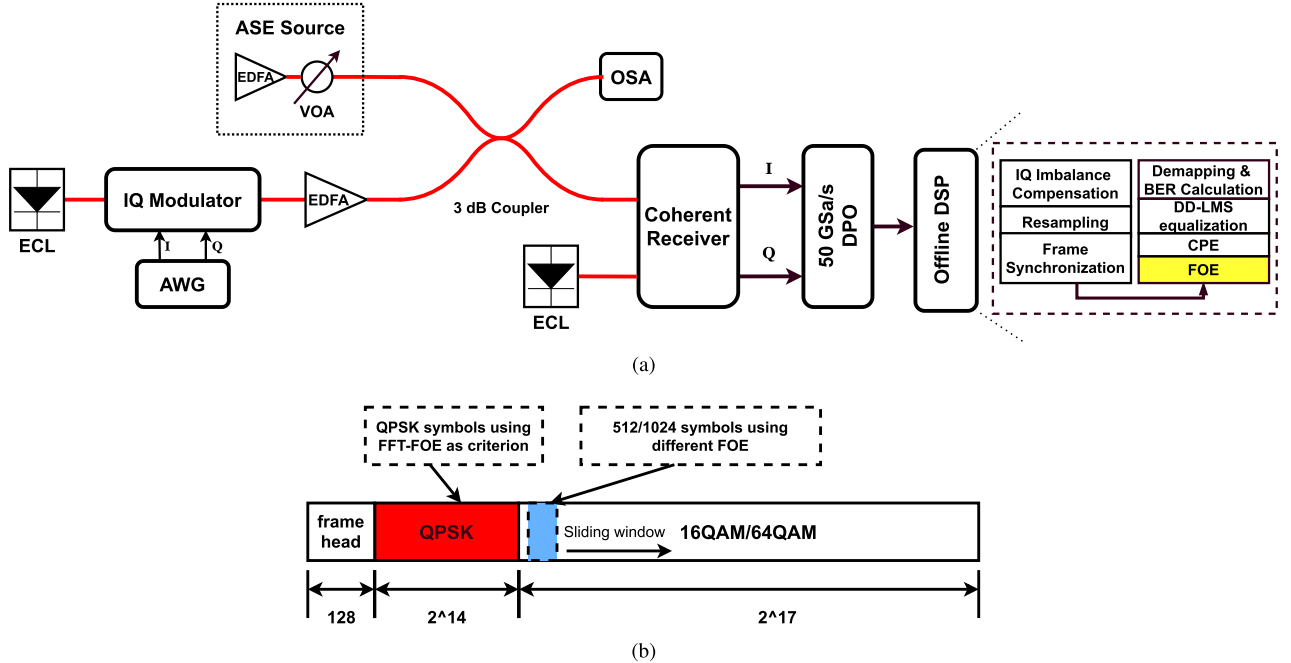

Fig. 6.   (a) Experimental setup and DSP flow for 20 GBaud 16/64-QAM system. (b) Frame structure.

bound (CRLB) is also presented for comparison [20]. It can be seen that all frequency offset estimators in the paper, including our proposed one, are biased. In the case of low SNR, a lot of estimation errors will occur due to the outliers effect for all FOE schemes [21]. Thus, the FOE schemes can only work effectively in the condition that SNR is greater than the threshold, and the SNR threshold can be reduce by increasing the FFT size in the FOE schemes. When SNR is greater the threshold, APFFT-FOE and the two-stage FOE can significantly reduce the bias, making the MSE drop by nearly an order of magnitude compared with FFT-FOE.

IV. EXPERIMENTAL SETUP AND RESULTS

To further validate the proposed FOE scheme, we carried out 20 GBaud 16/64-QAM experiments under BTB transmission as shown in Fig. 6(a). At the transmitter side, an external cavity laser (ECL) at 1550 nm with 25 kHz linewidth was used as transmitter source. The ECL and a 20 GBaud electrical 16/64-QAM signal generated by an arbitrary waveform generator (AWG) were fed into an optical IQ modulator. Then, the optical signal

was amplified to 0 dBm by an erbium-doped fiber amplifier (EDFA). An EDFA and a variable optical attenuator (VOA) was deployed as ASE noise source to adjust the optical SNR (OSNR). The OSNR of signal was monitored by optical spectrum analyzer (OSA). At the receiver side, another ECL with 25 kHz linewidth was used as the LO, and the setting of FO was realized by adjusting the central frequency of LO. Finally, the electrical signals after coherent detection were sampled by a 50GSa/s digital phosphor oscilloscope (DPO). In the offline DSP, after IQ imbalance compensation, resampling and frame synchronization, the FO was estimated by different FOE schemes. The FFT size in FFT-FOE or APFFT-FOE was set to 512/1024 for 16/64-QAM, and the parameter settings of the other two-stage FOE algorithm are consistent with the simulation. Then, after the blind phase search (BPS) based carrier phase estimation (CPE) bundled with the decision directed-least mean square (DD-LMS) equalization, and de-mapping/coding, the BER was measured. Fig. 6(b) shows the frame structure in the experiment. Similar to [13], the frame head was used for frame synchronization. The 16384 QPSK symbols were used to calculate the FO using FFT-FOE as the evaluation criterion. Due to the fact that the laser
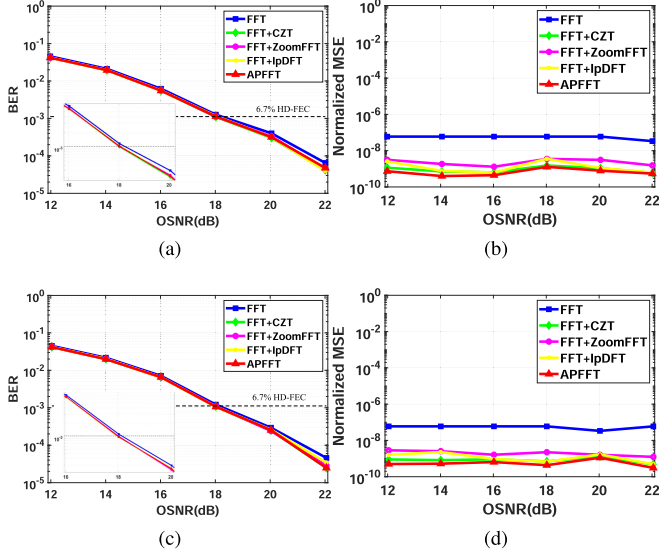
Fig. 7. BER and Normalized MSE as a function of OSNR for 20 GBaud 16-QAM signal, (a), (b) FO = 0 GHz, (c), (d) FO=2.3 GHz.

Fig. 8. BER and Normalized MSE as a function of OSNR for 20 GBaud 64-QAM signal, (a), (b) FO=0 GHz, (c), (d) FO=2.3 GHz.

frequency drifts with time at a speed of MHz/s in the experiment, while the duration of a frame of signal is on the order of ms, we can hold that the FO is consistent within a frame of signal.

Figs. 7(b) and (d) show the normalized MSE of different FOE schemes versus OSNR for 16-QAM signal with the FO to be 0 GHz and 2.3 GHz, respectively. The MSE of APFFT-FOE is around 7e-10, while that of FFT-FOE is around 5e-8. The decline of MSE is more than an order of magnitude. Fig. 7(a) and (c) depict the BER performance versus OSNR for 16-QAM signal under the same FO settings. We find that the APFFT-FOE has the same BER performance as the two-stage FOE over the entire OSNR range, and leads to 0.30 dB or 0.23 dB OSNR improvement at 6.7% HD-FEC threshold (BER=1.12e-3) compared with the FFT-FOE.

Fig. 8 show the BER performance and the normalized MSE as a function of OSNR for 64-QAM signal with the same FO setting as Fig. 7. Compared with the FFT-FOE, APFFT-FOE also reduces the MSE by more than one order of magnitude, from about 1.5e-8 to 5.5e-10. Similarly, no BER difference can be observed between APFFT-FOE and the two-stage FOE. However, compared with the FFT-FOE, APFFT-FOE can relax the required OSNR at 20% SD-FEC threshold (BER=2e-2) by 1.14 dB or 0.68 dB. This result indicates that the BER performance improvement due to the high estimation accuracy of FO is more obvious in higher order modulation.

Figs. 9(a) and 9(b) show the BER performance versus FO at a range of [-3 GHz, +3GHz] for 16-QAM and 64-QAM, respectively. All the FOE schemes have the same estimated range of [-2.5 GHz, +2.5GHz]. For the FO setting within the estimated range, the FFT-FOE always has a residual FO of $\frac{1}{8}\Delta f_{\text{res}}$ due to the picket-fence effect of FFT. The APFFT-FOE and the two-stage FOE have better BER performance due to its high precision FO estimation.

Based on the experimental results above, APFFT-FOE can improve the accuracy of FO estimation and achieve better BER
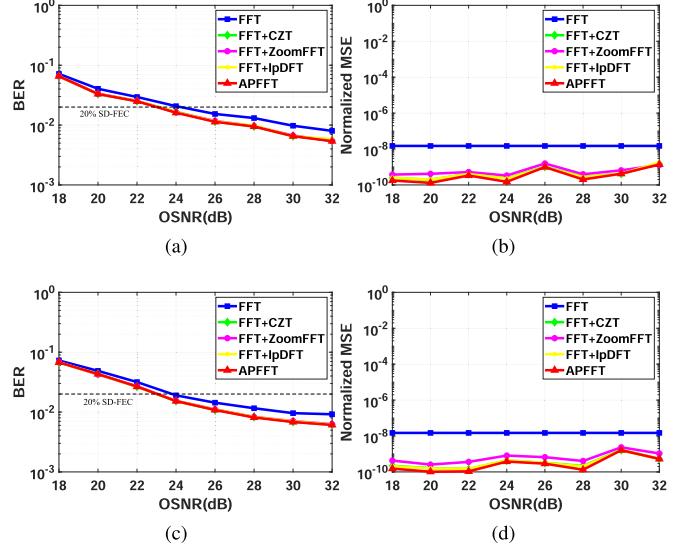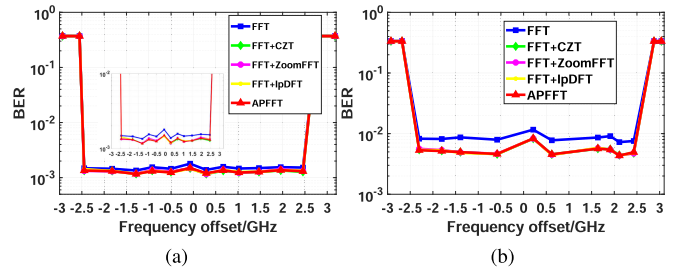

Fig. 9. BER with respect to various FO for (a) 16-QAM and (b) 64-QAM.

performance for 16/64-QAM signal compared with FFT-FOE, which achieves the same effect as the two-stage FOE. However, the additional computational complexity of APFFT-FOE is far below that of the two-stage FOE, which will be discussed in the next.

V. COMPLEXITY ANALYSIS

The complexity of DSP algorithm is crucial for practical application. Next, we analyze the computational complexity (CC) by compare the real multiplications of the three FOE schemes in the second step.

According to [16], the number of real multiplications of the N_2-point Zoom-FFT is

$$CC_{\text{Zoom-FFT}} = 2N_2 log_2 N_2 + 8N_1 \quad (11)$$

For M-point CZT of N_3 signals, the number of real multiplications can be express as [15]

$$CC_{\text{CZT}} = \left(\frac{106}{9} + \frac{4}{3}\log_2 N_1 + 2log_2 M\right) \times N_1 + (-1)^{log_2 N_1} - 8M \quad (12)$$

where $M = 32$, $N_1 = N_3 + M - 1$, and the split-radix FFT is used.

TABLE I
MULTIPLICATION COMPLEXITY

	CC_{CZT}	$CC_{Zoom\text{-}FFT}$	$Max\ CC_{IpDFT}$	CC_{APFFT}
16QAM	17051	8192	4116	2057
64QAM	35713	17408	8212	4105

As for the IpDFT method, The number of real multiplications is related to the value of the decimal part δ[17].

$$CC_{IpDFT} = \begin{cases} 10 & |\hat{\delta}| > 0.3 \\ 8N + 20 & |\hat{\delta}| \leq 0.3 \end{cases} \qquad (13)$$

when δ is less than 0.3, the discrete time Fourier transform (DTFT) performed by the algorithm requires a lot of computational complexity.

For our proposed APFFT-FOE, it takes $2 \times (2N_1 - 1)$ real multiplications to windowing the signal and a remainder operation to calculate δ beside the traditional FFT-FOE process. The remainder operation requires one multiplication and one division, and one division is equivalent to ten multiplications using Anderson-Earle-Goldschmidt-Powers algorithm. Finally, the number of real multiplications required by APFFT-FOE is

$$CC_{APFFT} = 2 \times (2N_1 - 1) + 11 \qquad (14)$$

The complexity of the three FOE schemes in the second step for 16/64-QAM are summarized in Table I. Compared with CZT, Zoom-FFT, IpDFT, the additional complexity of our proposed APFFT-FOE is reduced by about 87.9%, 74.9%, 50% for 16QAM and 88.7%, 76.4%, 50% for 64QAM, respectively.

VI. CONCLUSION

In this paper, we proposed a novel FOE scheme based on APFFT for M-QAM coherent optical systems, which has advantages of high FO estimation accuracy and low complexity. APFFT-FOE replaces the conventional FFT with APFFT, and correcting the estimation of FO using the APFFT phase spectrum. Simulation results show that APFFT-FOE can reduce the MSE of FO estimation by more than one order of magnitude compared with the conventional FFT-FOE, and has similar performance with the two-stage FOE basd on CZT, Zoom-FFT and IpDFT. However, the additional computational complexity of APFFT-FOE is reduced by more than 87%, 74% and 50% compared with the CZT, Zoom-FFT and IpDFT based algorithms, respectively. The experimental results by BTB transmission system using 20 GBaud 16/64-QAM signal indicate that APFFT-FOE can conduct to a better BER performance. In particular, APFFT-FOE reduces the required OSNR by 0.23 dB for 16-QAM at 6.7% HD-FEC threshold, and 0.68 dB for 64-QAM at 20% SD-FEC threshold.

REFERENCES

[1] I. Tomkos, S. Azodolmolky, J. Solé-Pareta, D. Careglio and E. Palkopoulou, "A tutorial on the flexible optical networking paradigm: State of the art, trends, and research challenges," *Proc. IEEE*, vol. 102, no. 9, pp. 1317–1337, Sep. 2014.

[2] H. Khodakarami, B. S. G. Pillai, B. Sedighi, and W. Shieh, "Flexible optical networks: An energy efficiency perspective," *J. Lightw. Technol.*, vol. 32, no. 21, pp. 3958–3969, 2014.

[3] P. J. Winzer, "High-spectral-efficiency optical modulation formats," *J. Lightw. Technol.*, vol. 30, no. 24, pp. 3824–3835, 2012.

[4] X. Zhou and L. Nelson, "Advanced DSP for 400 Gb/s and beyond optical networks," *J. Lightw. Technol.*, vol. 32, no. 16, pp. 2716–2725, 2014.

[5] H. Sun et al., "800G DSP ASIC design using probabilistic shaping and digital sub-carrier multiplexing," *J. Lightw. Technol.*, vol. 38, no. 17, pp. 4744–4756, 2020.

[6] J. Lu et al., "Joint carrier phase and frequency-offset estimation with parallel implementation for dual-polarization coherent receiver," *Opt. Exp.*, vol. 25, no. 5, 2017, Art. no. 5217.

[7] A. Leven, N. Kaneda, U. V. Koc, and Y. K. Chen, "Frequency estimation in intradyne reception," *IEEE Photon. Technol. Lett.*, vol. 19, no. 6, pp. 366–368, Mar. 2007.

[8] I. Fatadin and S. J. Savory, "Compensation of frequency offset for 16-QAM optical coherent systems using QPSK partitioning," *IEEE Photon. Technol. Lett.*, vol. 23, no. 17, pp. 1246–1248, Sep. 2011.

[9] Y. Liu, Y. Peng, Y. Zhang, Y. Liu, and Z. Zhang, "Differential phase-based frequency offset estimation for 16-QAM coherent optical systems," *IEEE Photon. Technol. Lett.*, vol. 26, no. 24, pp. 2492–2494, Dec. 2014.

[10] J. Lu et al., "Frequency offset estimation for 32-QAM based on constellation rotation," *IEEE Photon. Technol. Lett.*, vol. 29, no. 23, pp. 2115–2118, Dec. 2017.

[11] T. Yang et al., "Hardware-efficient multi-format frequency offset estimation for M-QAM coherent optical receivers," *IEEE Photon. Technol. Lett.*, vol. 30, no. 18, pp. 1605–1608, Sep. 2018.

[12] M. Selmi, Y. Jaouën, and P. Ciblat, "Accurate digital frequency offset estimator for coherent PolMux QAM transmission systems," in *Proc. Eur. Conf. Opt. Commun.*, 2009, pp. 1–2.

[13] F. Xiao et al., "Feed-forward frequency offset estimation for 32-QAM optical coherent detection," *Opt. Exp.*, vol. 25, no. 8, 2017, Art. no. 8828.

[14] A. Meiyappan, P. Y. Kam, and H. Kim, "On decision aided carrier phase and frequency offset estimation in coherent optical receivers," *J. Lightw. Technol.*, vol. 31, no. 13, pp. 2055–2069, 2013.

[15] H. Leng et al., "Frequency offset estimation for optical coherent M-QAM detection using chirp Z-transform," *IEEE Photon. Technol. Lett.*, vol. 24, no. 9, pp. 787–789, May 2012.

[16] B. Tang et al., "Low complexity two-stage FOE using modified Zoom-FFT for coherent optical M-QAM systems," *IEEE Photon. Technol. Lett.*, vol. 32, no. 5, pp. 263–266, Mar. 2020.

[17] J. Xiao et al., "Low complexity FFT-based frequency offset estimation for M-QAM coherent optical systems," *IEEE Photon. Technol. Lett.*, vol. 27, no. 13, pp. 1371–1374, Jul. 2015.

[18] X. Huang, Z. Wang, L. Ren, Y. Zeng, and X. Ruan, "A novel high-accuracy digitalized measuring phase method," in *Proc. Int. Conf. Signal Process. Proc.*, 2008, pp. 120–123.

[19] H. Xiaohong, W. Zhaohua, and H. Guoqiang, "New method of estimation of phase, amplitude, and frequency based on all phase FFT spectrum analysis," in *Proc. Int. Symp. Intell. Signal Process. Commun. Syst.*, 2007, pp. 284–287.

[20] G. Campobello, A. Segreto, and N. Donato, "A novel low-complexity frequency estimation algorithm for industrial Internet-of-Things applications," *IEEE Trans. Instrum. Meas.*, vol. 70, pp. 1–1, 2021, Art. no. 6501610, doi: 10.1109/TIM.2020.3035853.

[21] P. Ciblat and M. Ghogho, "Blind NLLS carrier frequency-offset estimation for QAM, PSK, and PAM modulations: Performance at low SNR," *IEEE Trans. Commun.*, vol. 54, no. 10, pp. 1725–1730, Oct. 2006.